ON THE INFINITE ORDER LIMIT OF HERMITE-BASED FINITE DIFFERENCE SCHEMES

DYLAN ABRAHAMSEN * AND BENGT FORNBERG †

Abstract. Pseudospectral (PS) methods are widely used for solving partial differential equations (PDEs) to high accuracy in simple geometries. They can be seen as the limit of finite difference (FD) methods for increasing order of accuracy. Similarly, recently introduced Hermite-based finite difference (HFD) approximations converge to Hermite-based pseudospectral (HPS) limits. We derive here HPS coefficients, and make comparisons between PS and HPS approximations. Using half the number of nodes and twice the amount of data per node, HPS approximations match the accuracy of the PS method. A potential advantage of HPS over PS arises when a computer has multiple cores available.

Key words. Hermite, pseudospectral, partial differential equations, initial value problem, finite differences

AMS subject classifications. Primary: 65M70 , Secondary: 65M06, 65T40

1 Introduction

Standard centered finite differences (FD) approximate a derivative at a grid point by a weighted combination of function values at adjacent grid points. The limits that the FD weights approach when such approximations are made increasingly accurate (and stencils wider) have been well documented [3]. In Hermite-type FD formulas, weights are assigned to both function and first derivative values in order to approximate some higher derivative (or to interpolate the function or a derivative of it). Following a recent fast algorithm for Hermite weights [4] and their application to PDEs (for the Korteweg-de Vries equation in [1]), the question arises if these weight sets, like those for regular FD methods, possess infinite order accurate limits. We find here that this indeed is the case. Pseudospectral implementations (using the FFT algorithm on periodic data) turn out to give particularly simple closed form expressions.

The limit formulas for regular FD weights on an infinite interval are briefly commented on in Section 2 before we turn to Hermite formulas in Section 3. We first carry over the FD limit derivation on an infinite interval to the HFD case in Section 3.1, and follow that in Section 3.2 with another derivation that gives additional insights in the HFD schemes. Section 3.3 presents an alternative closed form for FD and HFD weight limits. Section 4 discusses the periodic case, and is followed by numerical examples, conclusions, references, and an appendix with some FD, HFD, and HPS weight tables and further discussion.

2 Finite difference (FD) limits on an infinite interval

Following Appendix 2 in [2], the Lagrange interpolation polynomial for equispaced nodes x_i and data $f(x_i)$, $i = 1, 2, \ldots, N$ takes the form

$$L(x) = \sum_{i=1}^{N} L_i(x) \cdot f(x_i), \tag{2.1}$$

where

$$L_i(x) = \frac{\prod_{j=1, j\neq i}^{n}(x - x_j)}{\prod_{j=1, j\neq i}^{n}(x_i - x_j)}. \tag{2.2}$$

Choosing instead as nodes the doubly infinite sequence $x_i = k = \ldots, -2, -1, 0, 1, 2, \ldots$, it follows from the sine product $\frac{\sin \pi x}{\pi x} = \prod_{k=1}^{\infty} \left(1 - \left(\frac{x}{k}\right)^2\right)$ that, in this limit, $L_i(x)$ converges to $\frac{\sin \pi(x-k)}{\pi(x-k)}$, and we obtain the weights

$$w_k^{(p)} = \frac{d^p}{dx^p}\left(\frac{\sin \pi(x-k)}{\pi(x-k)}\right)\bigg|_{x=0} = (-1)^p \frac{d^p}{dx^p}\left(\frac{\sin \pi x}{\pi x}\right)\bigg|_{x=k}. \tag{2.3}$$

*Department of Applied Mathematics, University of Colorado, Boulder, CO 80309, USA : dylan.abrahamsen@colorado.edu
†Department of Applied Mathematics, University of Colorado, Boulder, CO 80309, USA : bengt.fornberg@colorado.edu

Some notable features of these FD weight limits include:

1. The weights always oscillate in sign as k moves away from $k = 0$,
2. For a odd order derivatives, the weights decay in magnitude as $O(1/|k|)$ while, for even order derivatives, the decay rate is faster, $O(1/|k|^2)$.

3 Hermite limits on an infinite interval

Looking at Table 7.2 in the Appendix, showing HFD weights, it is not immediately obvious that going down any of the columns (beyond order 16, towards infinite order) will produce convergent sequences. Another difference to the FD case is that the weights do not oscillate in sign as x moves away from $x = 0$. The next Sections 3.1 and 3.2 give two different ways to derive limit formulas for the Hermite weights. For simplicity of notation, we set the node spacing $h = 1$ in most of the following analysis.

3.1 HFD limits derived by means of infinite products

The derivation above of (2.3) generalizes quite straightforwardly to the HFD case, as shown next in Section 3.1.1.

3.1.1 Infinite product derivation in the HFD case

Instead of (2.1), the starting point is now

$$H(x) = \sum_{i=1}^{N} P_i(x) \cdot f(x_i) + \sum_{i=1}^{N} Q_i(x) \cdot f'(x_i), \tag{3.1}$$

where $P_i(x)$ and $Q_i(x)$ need to satisfy

$$P_i(x_k) = \begin{cases} 1, & k = i \\ 0, & k \neq i \end{cases} \quad \text{and} \quad P_i'(x_k) = 0$$
$$Q_i(x_k) = 0 \quad \text{and} \quad Q_i'(x_k) = \begin{cases} 1, & k = i \\ 0, & k \neq i \end{cases}$$

Following [4], the function $(L_i(x))^2$ satisfies all requirements for P_i except that $\frac{d(L_i(x))^2}{dx}\big|_{x=x_i} = 2\frac{dL_i(x)}{dx}\big|_{x=x_i} = 2\sum_{l\neq i} \frac{1}{x_i - x_l}$. The function $(x - x_i)\,(L_i(x))^2$ satifies all the requirements for $Q_i(x)$. Thus, we can write $P_i(x)$ and $Q_i(x)$ in terms of $L_i(x)$ as

$$P_i(x) = \left[1 - 2(x - x_i)L_i'(x_i)\right] L_i(x)^2$$
$$Q_i(x) = (x - x_i)\, L_i(x)^2$$

In the same limit as above, with $x_i = k = \ldots, -2, -1, 0, 1, 2, \ldots$, we obtain $P_k(x) \to \left(\frac{\sin \pi(x-k)}{\pi(x-k)}\right)^2$ and $Q_k(x) \to (x - k)\left(\frac{\sin \pi(x-k)}{\pi(x-k)}\right)^2$, from which follows

$$\frac{d^p}{dx^p} H(x)\bigg|_{x=0} = \sum_{k=-\infty}^{\infty} \frac{d^p}{dx^p} P_k(x)\bigg|_{x=0} \cdot f(x_k) + \sum_{k=-\infty}^{\infty} \frac{d^p}{dx^p} Q_k(x)\bigg|_{x=0} \cdot f'(x_k)$$

and

$$\frac{d^p}{dx^p} f(x)\bigg|_{x=0} \approx \sum_{k=-\infty}^{\infty} a_k^{(p)} \cdot f(x_k) + \sum_{k=-\infty}^{\infty} b_k^{(p)} \cdot f'(x_k) \tag{3.2}$$

with

$$a_k^{(p)} = (-1)^p \, \frac{d^p}{dx^p} \left(\frac{\sin \pi x}{\pi x}\right)^2 \bigg|_{x=k} \quad \text{and} \quad b_k^{(p)} = (-1)^{p+1} \, \frac{d^p}{dx^p} \left\{ x \left(\frac{\sin \pi x}{\pi x}\right)^2 \right\} \bigg|_{x=k}. \tag{3.3}$$

3.2 HFD limits by means of Fourier series expansions A key difference between FD and HFD approximations concerns the range of Fourier modes $\nu(x) = e^{i\omega x}$ these schemes can approximate, given a grid spacing h. For FD schemes, using function values only, any mode outside the range

$$-\frac{\pi}{h} \leq \omega \leq +\frac{\pi}{h} \tag{3.4}$$

is, due to aliasing, indistinguishable from a mode within this range. For an HFD scheme, picking up h-spaced information of both $\nu(x) = e^{i\omega x}$ and $\nu'(x) = i\omega e^{i\omega x}$, the range becomes doubled [1], to

$$-\frac{2\pi}{h} \leq \omega \leq +\frac{2\pi}{h}, \tag{3.5}$$

as shown in Figure 5.4. This range doubling can be explained in part by dispersion analysis shown in [1] and briefly in the Appendix of this paper.

To keep the notation simple, the following derivation is for the derivative order $p = 4$, but it generalizes to any order. In the notation used in (3.2) (with h=1), the limiting weights for the function values are $a_k^{(4)}$ and for the first derivative values $b_k^{(4)}$, k integer, i.e.,

$$f^{(4)}(0) \approx \sum_{k=-\infty}^{\infty} a_k^{(4)} f(k) + \sum_{k=-\infty}^{\infty} b_k^{(4)} f'(k), \tag{3.6}$$

Based on the patterns seen in Table 7.2, we expect the $a_k^{(4)}$ sequence to be symmetric about $k = 0$ and the $b_k^{(4)}$ sequence anti-symmetric, making it sufficient to find $a_k^{(4)}$ for $k = 0, 1, 2, 3, \ldots$ and $b_k^{(4)}$ for $k = 1, 2, 3, \ldots$. This can also be more technically explained via the symmetry of the grid around $k = 0$ and requiring that the stencil is accurate for all polynomial powers x^p. Applying these limiting weights to $e^{i\omega x}$, we expect (based on the comments just above) that

$$\omega^4 = a_0^{(4)} + 2\sum_{k=1}^{\infty} a_k^{(4)} \cos k\omega - 2\omega \sum_{k=1}^{\infty} b_k^{(4)} \sin k\omega = a_0 + 2S_1(\omega) - 2\omega S_2(\omega) \tag{3.7}$$

holds for all ω in the range $-2\pi < \omega < +2\pi$. The two functions $S_1(\omega)$ and $S_2(\omega)$ are both $[-\pi, \pi]$-periodic. The question becomes how one then can get (3.7) to hold exactly over a twice as wide interval $(-2\pi, 2\pi)$. The next two subsections show (i) an explicit construction leading to closed form expressions for the $\{a_k^{(4)}\}$ and $\{b_k^{(4)}\}$ sequences, and (ii) that these coefficients are uniquely determined.

3.2.1 Explicit construction of the coefficient sequences We start by noting that there is a unique way to split ω^4 over the interval $[0, 2\pi]$

$$\omega^4 = P_1(\omega) + \omega P_2(\omega)\,, \tag{3.8}$$

if we require that $P_1(\omega)$ is symmetric and $P_2(\omega)$ is anti-symmetric around $\omega = \pi$:

$$\begin{aligned} P_1(\omega) &= -3\omega^4 + 12\pi\omega^3 - 16\pi^2\omega^2 + 8\pi^3\omega \\ P_2(\omega) &= 4\omega^3 - 12\pi\omega^2 + 16\pi^2\omega - 8\pi^3 \end{aligned} \tag{3.9}$$

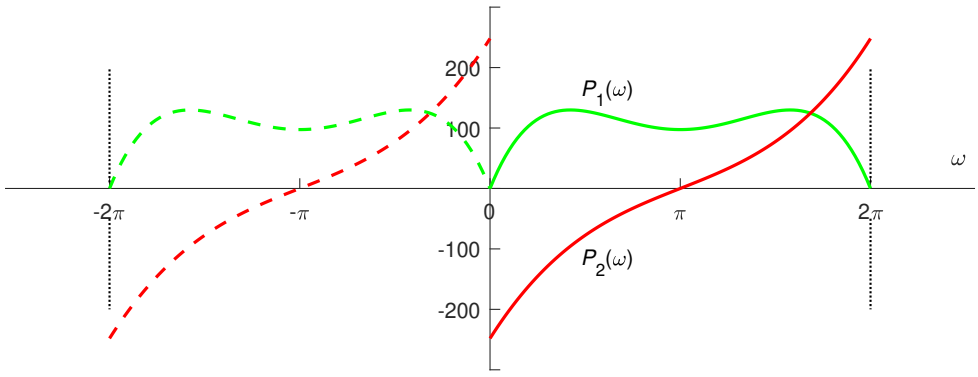

Fig. 3.1: The functions $P_1(\omega)$ and $P_2(\omega)$, as defined in (3.9) and extended across $\omega = 0$.

Figure 3.1 illustrates these two functions, as solid curves over $[0, 2\pi]$ and then also (as dashed curves over $[-2\pi, 0]$) their symmetric and anti-symmetric extensions, respectively, across $\omega = 0$. We next find the Fourier series coefficients for these functions as calculated over $[-\pi, \pi]$:

$$\begin{array}{lll} P_1(\omega) & = \frac{16\pi^4}{15} + & \sum_{k=1}^{\infty} \left(-\frac{16\pi^2}{k^2} + \frac{144}{k^4} \right) \cos k\omega \\ P_2(\omega) & = & \sum_{k=1}^{\infty} \left(-\frac{16\pi^2}{k} + \frac{48}{k^3} \right) \sin k\omega \end{array} \tag{3.10}$$

Looking at the symmetries that are apparent in Figure 3.1, it is clear that these Fourier expansions return the correct values for the $P_1(\omega)$ and $P_2(\omega)$ functions not just over $[-\pi, \pi]$ but also over the double interval $[-2\pi, 2\pi]$. Recalling (3.8), equating coefficients between (3.10) and (3.7) now gives the desired coefficients in (3.6):

$$\left\{ \begin{array}{ll} a_0^{(4)} & = \frac{16\pi^4}{15}, \\ a_k^{(4)} & = -\frac{8\pi^2}{k^2} + \frac{72}{k^4}, \quad k = 1, 2, 3, \ldots \\ b_0^{(4)} & = 0 \\ b_k^{(4)} & = \frac{8\pi^2}{k} - \frac{24}{k^3}, \quad k = 1, 2, 3, \ldots \end{array} \right. \tag{3.11}$$

3.2.2 Proof of uniqueness The construction in the previous Section 3.2.1 provided one set of expansion coefficients $\{a_k^{(4)}\}$ and $\{b_k^{(4)}\}$ such that

$$\omega^4 = a_0^{(4)} + 2 \sum_{k=1}^{\infty} a_k^{(4)} \cos k\omega - 2\omega \sum_{k=1}^{\infty} b_k^{(4)} \sin k\omega$$

is valid over $\omega \in (-2\pi, 2\pi)$. Suppose there is a different coefficient set with this same property. We then subtract the two cases, and denote the differences in the coefficients by $\{c_k^{(4)}\}$ and $\{d_k^{(4)}\}$, respectively. It then holds that

$$0 \equiv c_0^{(4)} + 2 \sum_{k=1}^{\infty} c_k^{(4)} \cos k\omega - 2\omega \sum_{k=1}^{\infty} d_k^{(4)} \sin k\omega.$$

If all $d_k^{(4)}$ coefficients are zero, so are the $c_k^{(4)}$ coefficients. Suppose next that at least one $d_k^{(4)}$ coefficient is nonzero, and divide by the last sum

$$2\omega \equiv \frac{c_0^{(4)} + 2 \sum_{k=1}^{\infty} c_k^{(4)} \cos k\omega}{\sum_{k=1}^{\infty} d_k^{(4)} \sin k\omega}. \tag{3.12}$$

The RHS in (3.12) is $(-\pi,\pi)$-periodic, and can therefore not match the LHS over $(-2\pi,2\pi)$. From this contradiction, we conclude that the $\{c_k^{(4)}\}$ and $\{d_k^{(4)}\}$ coefficients must be all zero, therefore (3.11) uniquely satisfies (3.7).

3.3 PS and HPS coefficients in closed form While (2.3) and (3.3) are of 'closed form', they can be re-expressed as finite sums with no derivatives required. For example, (3.3) in the case of $p=4$ evaluates to (3.11). We start by observing the p-th derivative product rule

$$\frac{d^p}{dx^p}\left[f(x)g(x)\right] = \sum_{n=0}^{p} \binom{p}{n} f^{(n)}(x) g^{(p-n)}(x). \tag{3.13}$$

By letting $f(x)=\sin \pi x$ and $g(x)=(\pi x)^{-1}$ the FD weights $w_k^{(p)} = (-1)^p \frac{d^p}{dx^p}\left(\frac{\sin \pi x}{\pi x}\right)\Big|_{x=k}$ (as given in (2.3)) can be expressed using (3.13) as

$$\begin{cases} w_0^{(p)} & = \cos\left(\frac{\pi p}{2}\right) \frac{\pi^p}{p+1} \\ w_k^{(p)} & = \sum_{n=1}^{p} (-1)^{p+n} \frac{\pi^{n-1} p! \sin\left(\pi\left(\frac{n}{2}+k\right)\right)}{n! k^{p-n+1}}, \quad k=\pm 1,\pm 2,\pm 3,\ldots \end{cases} \tag{3.14}$$

Similarly the weights defined in (3.3) can be expressed as

$$\begin{cases} a_0^{(p)} & = \cos\left(\frac{\pi p}{2}\right) \frac{(2\pi)^p}{\left(\frac{p}{2}+1\right)(p+1)} \\ a_k^{(p)} & = \sum_{n=1}^{\frac{p}{2}} (-1)^{p+n+1} \frac{2^{2n-1}\pi^{2n-2}(p-2n+1)p!}{(2n)! k^{p-2n+2}}, \quad k=\pm 1,\pm 2,\pm 3,\ldots \\ b_0^{(p)} & = \sin\left(\frac{\pi p}{2}\right) \frac{2^p \pi^{p-1}}{p+1} \\ b_k^{(p)} & = \sum_{n=1}^{\frac{p}{2}} (-1)^{p+n} \frac{2^{2n-1}\pi^{2n-2} p!}{(2n)! k^{p-2n+1}}, \quad k=\pm 1,\pm 2,\pm 3,\ldots \end{cases} \tag{3.15}$$

The special case when $p=2$:

$$\begin{cases} a_0^{(2)} & = -\frac{2\pi^2}{3} \\ a_k^{(2)} & = \frac{2}{k^2}, \qquad k=\pm 1,\pm 2,\pm 3,\ldots \\ b_0^{(2)} & = 0 \\ b_k^{(2)} & = -\frac{2}{k}, \quad k=\pm 1,\pm 2,\pm 3,\ldots \end{cases} \tag{3.16}$$

A list of coefficients for various fixed p is given in Table 7.3 of the Appendix.

4 Hermite limits in the periodic (PS) case

In this section we derive HPS weights on periodic domains using two approaches: (i) direct aliasing, and (ii) convolutions (to be used in conjunction with the fast Fourier transform (FFT)).

4.1 HPS weights via direct aliasing On the periodic interval $[-\pi,\pi]$ with N equispaced nodes at $x_i = \pi\left(\frac{2i}{N}-1\right)$ for $i=0,1,2,\cdots,N-1$ the infinitely wide FD stencil for the p-th derivative can be expressed in closed form [5] using aliasing as

$$\frac{d^p}{dx^p}\begin{bmatrix} u_0 \\ \vdots \\ u_{N-1} \end{bmatrix} = \begin{bmatrix} \quad \\ \quad W^{(p)} \quad \\ \quad \end{bmatrix} \begin{bmatrix} u_0 \\ \vdots \\ u_{N-1} \end{bmatrix}. \tag{4.1}$$

When N is even the closed form for the first two derivatives are,
$p=1$:

$$W_{i,j}^{(1)} = \begin{cases} 0 & \text{if } i=j \\ \frac{(-1)^{i-j}}{2} \cot\frac{(i-j)h}{2} & \text{otherwise} \end{cases}$$

and $p = 2$:

$$W_{i,j}^{(2)} = \begin{cases} -\frac{\pi^2}{3h^2} - \frac{1}{6} & \text{if } i = j \\ (-1)^{i-j+1} \csc^2\left(\frac{(i-j)h}{2}\right) & \text{otherwise} \end{cases}$$

where h is the node spacing. Closed forms are available for N odd as well [8].

The extension of (4.1) to HFD on the periodic interval $[0, N]$ with N unit spaced nodes becomes

$$\frac{d^p}{dx^p}\begin{bmatrix} u_0 \\ \vdots \\ u_{N-1} \end{bmatrix} = \begin{bmatrix} \\ \mathbf{C^{(p)}} \\ \\ \end{bmatrix}\begin{bmatrix} u_0 \\ \vdots \\ u_{N-1} \end{bmatrix} + \begin{bmatrix} \\ \mathbf{D^{(p)}} \\ \\ \end{bmatrix}\begin{bmatrix} u_0' \\ \vdots \\ u_{N-1}' \end{bmatrix}. \tag{4.2}$$

where the elements of $\mathbf{C^{(p)}}$ and $\mathbf{D^{(p)}}$ can be found by similarly aliasing (3.15). The periodic interval $[0, N]$ rather than $[-\pi, \pi]$ is chosen to simplify the expressions shown in (4.3). Since $\mathbf{C^{(p)}}$ and $\mathbf{D^{(p)}}$ are symmetric circulant matrices it suffices to only find the first row. We note that $\left.\frac{d^{(p)}u}{dx^{(p)}}\right|_{x=0} = \sum_{k=0}^{N-1} c_k^{(p)} u(k) + d_k^{(p)} u'(k)$ where $c_k = \sum_{n=-\infty}^{\infty} a_{k+nN}^{(p)}$ and $d_k = \sum_{n=-\infty}^{\infty} b_{k+nN}^{(p)}$. These aliased coefficients $c_k^{(p)}$ and $d_k^{(p)}$ can be written in closed form as

$$\begin{cases} c_0^{(p)} = \cos\left(\frac{\pi p}{2}\right) \frac{(2\pi)^p}{\left(\frac{p}{2}+1\right)(p+1)} + \sum_{m=1}^{\frac{p}{2}} (-1)^{m+1} \left[(-1)^p + 1\right] \frac{2^{2m-1}\pi^{2m-2}(p-2m+1)p!}{(2m)!N^{p-2m+2}} \zeta(p-2m+2) \\ c_k^{(p)} = \sum_{m=1}^{\frac{p}{2}} (-1)^{p+m+1} \frac{2^{2m-1}\pi^{2m-2}(p-2m+1)p!}{(2m)!} \sum_{n=-\infty}^{\infty} \frac{1}{(k+nN)^{p-2m+2}}, \quad k = 1, 2, \ldots, N-1 \end{cases}$$
$$\begin{cases} d_0^{(p)} = \sin\left(\frac{\pi p}{2}\right) \frac{2^p \pi^{p-1}}{p+1} + \sum_{m=1}^{\frac{p}{2}} (-1)^m \left[(-1)^p - 1\right] \frac{2^{2m-1}\pi^{2m-2}p!}{(2m)!N^{p-2m+1}} \zeta(p-2m+1) \\ d_k^{(p)} = \sum_{m=1}^{\frac{p}{2}} (-1)^{p+m} \frac{2^{2m-1}\pi^{2m-2}p!}{(2m)!} \sum_{n=-\infty}^{\infty} \frac{1}{(k+nN)^{p-2m+1}}, \quad k = 1, 2, \ldots, N-1 \end{cases} \tag{4.3}$$

where $\zeta(s)$ is the Zeta function. While these forms in (4.3) seem cumbersome they simplify into very manageable forms for fixed p values. For example the $p = 2$ case:

$$\begin{cases} c_0^{(2)} = \frac{2\pi^2}{3}\left(\frac{1}{N^2} - 1\right) \\ c_k^{(2)} = \frac{2\pi^2 \csc^2 \frac{k\pi}{N}}{N^2}, \quad k = 1, 2, \ldots, N-1 \end{cases}$$
$$\begin{cases} d_0^{(2)} = 0 \\ d_k^{(2)} = -\frac{2\pi \cot \frac{k\pi}{N}}{N}, k = 1, 2, \ldots, N-1 \end{cases} . \tag{4.4}$$

One immediate benefit of the Hermite construction is the single form for either N even or odd as opposed to the FD counterpart where the two cases need to be treated separately. Table 7.3 in the Appendix shows weights for several fixed p values.

4.2 HPS weights via convolution When N is small, (4.1) and (4.2) can be computed quickly by simple matrix × vector multiplication. However, when N becomes large, a faster option is convolution via the fast Fourier transform (FFT). The digonalization can be explained by again noting $\mathbf{C^{(p)}}$ and $\mathbf{D^{(p)}}$ are symmetric circulant matrices. On the periodic interval $[0, N]$ with $N-1$ unit-spaced nodes (4.2) can instead be written

$$\frac{d^p}{dx^p}\begin{bmatrix} u_0 \\ \vdots \\ u_n \end{bmatrix} = \left[\mathbf{U}\right]\begin{bmatrix} \hat{c}_0^{(p)} & & \\ & \ddots & \\ & & \hat{c}_{N-1}^{(p)} \end{bmatrix}\left[\mathbf{U}^{-1}\right]\begin{bmatrix} u_0 \\ \vdots \\ u_n \end{bmatrix} + \left[\mathbf{U}\right] i \begin{bmatrix} \hat{d}_0^{(p)} & & \\ & \ddots & \\ & & \hat{d}_{N-1}^{(p)} \end{bmatrix}\left[\mathbf{U}^{-1}\right]\begin{bmatrix} u_0' \\ \vdots \\ u_n' \end{bmatrix} \tag{4.5}$$

where $\left[\mathbf{U}\right]$ is the direct Fourier transform (DFT) matrix, with elements $U_{k,l} = e^{\frac{2\pi ikl}{N}}$, $0 \le k,l \le N-1$. After multiplying with $\left[\mathbf{U}^{-1}\right]$ from the left

$$\left[\mathbf{U}^{-1}\right] \frac{d^p}{dx^p} \begin{bmatrix} u_0 \\ \vdots \\ u_n \end{bmatrix} = \begin{bmatrix} \hat{c}_0^{(p)} & & \\ & \ddots & \\ & & \hat{c}_{N-1}^{(p)} \end{bmatrix} \left[\mathbf{U}^{-1}\right] \begin{bmatrix} u_0 \\ \vdots \\ u_n \end{bmatrix} + i \begin{bmatrix} \hat{d}_0^{(p)} & & \\ & \ddots & \\ & & \hat{d}_{N-1}^{(p)} \end{bmatrix} \left[\mathbf{U}^{-1}\right] \begin{bmatrix} u_0' \\ \vdots \\ u_n' \end{bmatrix}. \tag{4.6}$$

The Fourier modes representable on the grid (in view of aliasing) are $e^{2\pi ixk/N}$ up through $|k| \approx \frac{N}{2}$. We do however look for HPS formulas that are exact up through $|k| \approx N$. We consider a k in the smaller range, and expect the correct result also for mode $k-N$. We next note (i) when inserting a single Fourier mode for the vector u, (4.5) reduces to one single nontrivial line (all others becoming zero), and (ii) on the grid, the scheme cannot tell the difference between the two modes k and $k-N$. We thus obtain for the two modes

$$\begin{array}{lccc} 0^{\text{th}} \text{ deriv.} & e^{2\pi ixk/N} & \& & e^{2\pi ix(k-N)/N} \\ 1^{\text{st}} \text{ deriv.} & \left(\frac{2\pi ik}{N}\right) e^{2\pi ixk/N} & \& & \left(\frac{2\pi i(k-N)}{N}\right) e^{2\pi ix(k-N)/N} \\ \vdots & \vdots & & \vdots \\ p^{\text{th}} \text{ deriv.} & \left(\frac{2\pi ik}{N}\right)^p e^{2\pi ixk/N} & \& & \left(\frac{2\pi i(k-N)}{N}\right)^p e^{2\pi ix(k-N)/N} \end{array}$$

Both of these cases k and $k-N$ contribute to line k in (4.6), giving respectively

$$\begin{aligned} \left(\tfrac{2\pi ik}{N}\right)^p &= i\hat{d}_k^{(p)} \left(\tfrac{2\pi ik}{N}\right) + \hat{c}_k^{(p)}, \\ \left(\tfrac{2\pi i(k-N)}{N}\right)^p &= i\hat{d}_k^{(p)} \left(\tfrac{2\pi i(k-N)}{N}\right) + \hat{c}_k^{(p)} \end{aligned}.$$

Solving for the coefficients give

$$\begin{cases} \hat{c}_k^{(p)} &= (2\pi)^{p-1} \left[\left(\frac{ik}{N}\right)^p - \left(\frac{i(k-N)}{N}\right)^p \right] \\ \hat{d}_k^{(p)} &= \frac{(2\pi)^p}{N} \left[(N-k) \left(\frac{ik}{N}\right)^p + k \left(\frac{i(k-N)}{N}\right)^p \right] \end{cases} \quad k = 0, 1, 2, \ldots, N-1. \tag{4.7}$$

In particular the $p = 2$ case, this becomes

$$\begin{cases} \hat{c}_k^{(2)} &= \frac{4k(k-N)\pi^2}{N^2} \\ \hat{d}_k^{(2)} &= \left(\frac{4k}{N} - 2\right)\pi \end{cases} \quad k = 0, 1, 2, \ldots, N-1. \tag{4.8}$$

Table 7.3 in the Appendix contain the convolution weights for various fixed p. Note that in these formulas (as opposed to in (4.3) and (4.4)), $k = 0$ need not be treated as a separate case from $k \neq 0$.

5 Numerical illustrations

In this section we present numerical findings when using HPS to discretize in space. Section 5.1 discusses the convergence of HFD weights to the HPS coefficients. In Section 5.2 the accuracy of HPS is tested on several functions with various levels of 'smoothness'. Section 5.3 details the dispersion of FD and HFD stencils in comparison with PS and HPS. Section 5.4 comments on time stepping stability constraints. For these sections we consider the 1-D transport equation

$$\frac{\partial u}{\partial t} + \frac{\partial u}{\partial x} = 0. \tag{5.1}$$

In order to apply HFD or HPS, the PDE must first be differentiated once in space [1]. Letting $u_x = v$ the PDE can be expressed as the system

$$\begin{bmatrix} u \\ v \end{bmatrix}_t = - \begin{bmatrix} v \\ u_{xx} \end{bmatrix}. \tag{5.2}$$

In Section 5.5, we consider a variable coefficient counterpart to (5.1).

5.1 Convergence of HFD weights The second derivative operator in (5.2) can be effectively approximated by HFD. In the limit as the stencil width (s.w.) of HFD becomes infinitely wide we expect the weights to converge to (3.16). Figure 5.1 shows how quickly HFD weights converge to the infinite interval HPS coefficients ($a_k^{(2)}$ and $b_k^{(2)}$) as s.w. increases. Only the first ten coefficients are considered while the limit determined by (3.16) is shown in gray. For graphical clarity only the magnitude of the weights are shown.

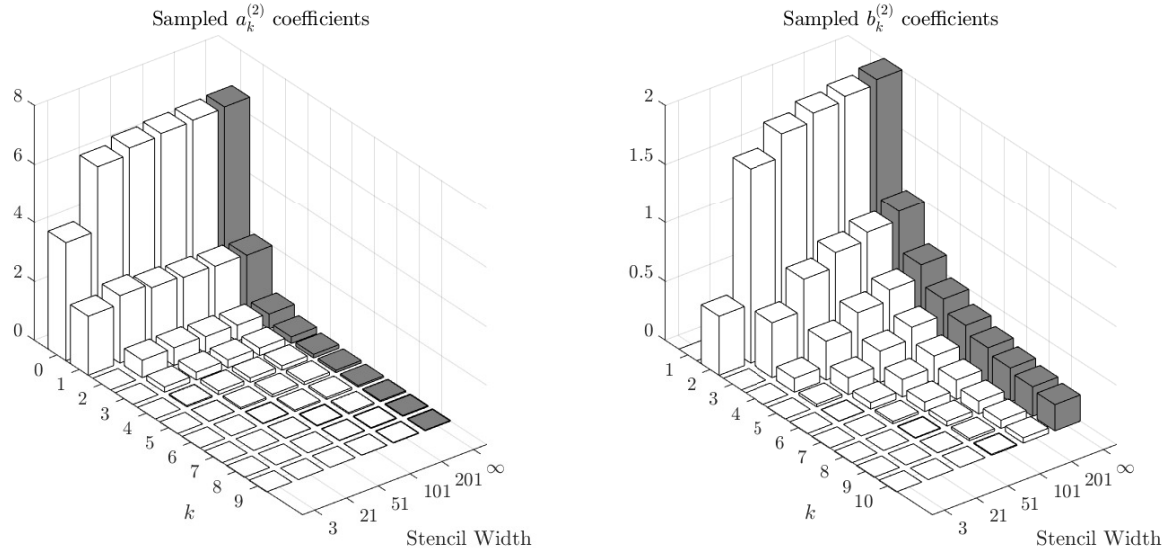

Fig. 5.1: The first ten HFD weights for (left) $a_k^{(2)}$, function values, and (right) $b_k^{(2)}$, derivative values, compared to their respective infinite interval HPS coefficients at different stencil sizes.

In this case of approximating an even order derivative (here $p = 2$), the coefficients acting on function values decay like $\mathcal{O}\left(\frac{1}{k^2}\right)$ rather than $\mathcal{O}\left(\frac{1}{k}\right)$ when using PS to solve (5.1). This implies HPS is more 'locally' influenced by function values over its PS counterpart. While PS alternates between $\mathcal{O}\left(\frac{1}{k}\right)$ and $\mathcal{O}\left(\frac{1}{k^2}\right)$ decay rates as p increases, HPS alternates between $\mathcal{O}\left(\frac{1}{k^2}\right)$ and $\mathcal{O}\left(\frac{1}{k^3}\right)$ for the coefficients acting on function values. These HPS decay rates can be found explicitly via (3.15) for all values of p or for select values in Table 7.3 in the appendix.

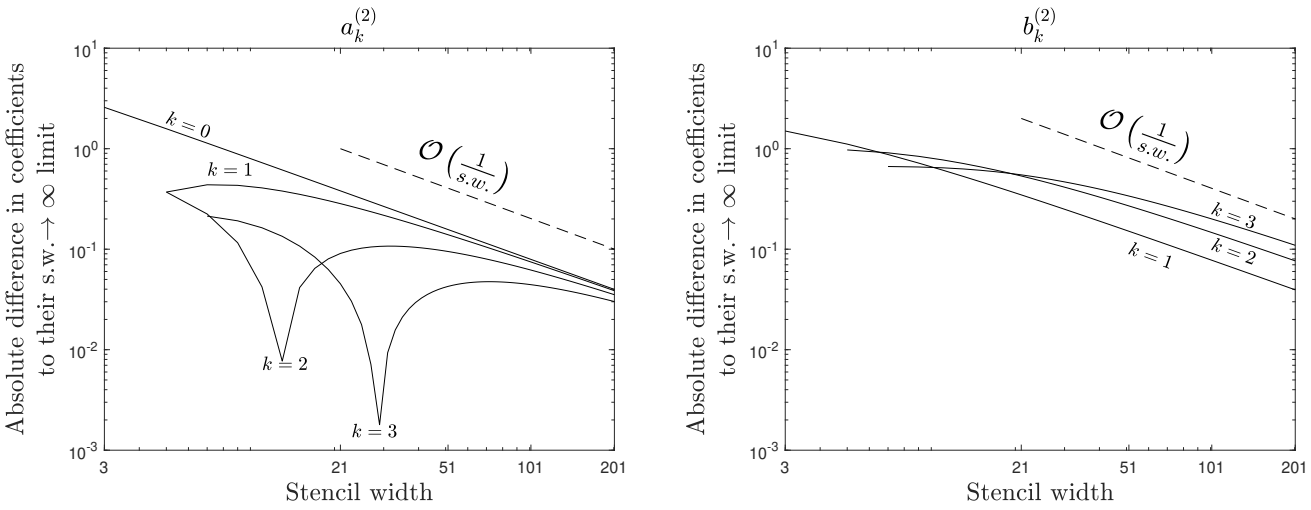

Fig. 5.2: The convergence of the first four HFD weights for (left) $a_k^{(2)}$, function values, and (right) $b_k^{(2)}$, derivative values, to their respective infinite interval HPS coefficients.

Figure 5.2 shows the rate at which the first four HFD coefficients $a_k^{(2)}$ and $b_k^{(2)}$ convergence to their respective HPS coefficients in (3.16). The convergence rate seems to eventually become $\mathcal{O}\left(\frac{1}{\text{s.w.}}\right)$ for all k. The $k=0$ case is excluded from the $b_k^{(2)}$ plot due to always having a value of zero.

5.2 Accuracy The 'smoothness' of a function will dictate the convergence rate when using standard PS for differentiation [7]. Since only the first derivative is utilized in (5.1) and the second derivative in (5.2) it is of interest to compare convergence rates. We consider four different periodic test functions - (i) $|\sin(x)|^3$, (ii) $\exp\left(-\sin^{-2}\left(\frac{x}{2}\right)\right)$, (iii) $\left(1+\sin^2\left(\frac{x}{2}\right)\right)^{-1}$, and (iv) $\sin(10x)$, similar to the convergence rate test in [7].

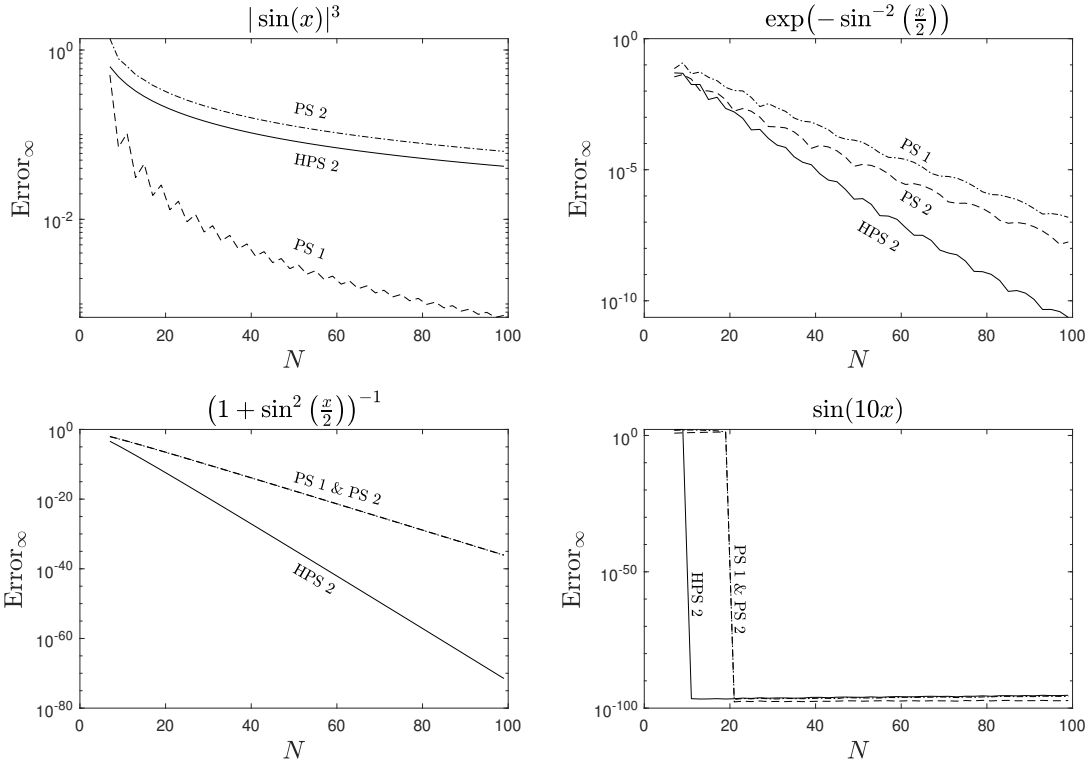

Fig. 5.3: A comparison of convergence rates for the first derivative using PS (PS 1) and for the second derivative using PS (PS 2) and HPS (HPS 2) on several periodic functions as a function on N.

Figure 5.3 compares the convergence rates for PS ($p = 1$ and $p = 2$) with HPS for $p = 2$ for the periodic test functions. For a given N, the HPS $p = 2$ approximation features roughly double as many correct digits as the PS $p = 2$ approximation, as expected since it uses double the amount of information at each node (both function and first derivative values). In some cases the HPS $p = 2$ approximation features roughly double as many digits as the PS $p = 1$ case. For functions with discontinuous first derivatives (like $|\sin(x)|^3$) we expect second derivative approximations to often be worse than first derivative approximations. However, when the function is smooth enough to be expressed as a finite sum of Fourier modes (like $\sin(10x)$) HPS will reach the threshold to exactly approximate the derivatives at half the nodes compared to PS. This is discussed more in Section 5.3. All extended precision calculations were done with the Advanpix package [6].

5.3 Dispersion The single Fourier mode solution to (5.1) is $u(x,t) = e^{i\omega x - i\alpha(\omega)t}$ where analytically $\alpha(\omega) = \omega$. Discretizing in space and plugging this solution into either (5.1) or (5.2) (depending on using FD/PS or HFD/HFD respectively) yields a method of analysing dispersion [1].

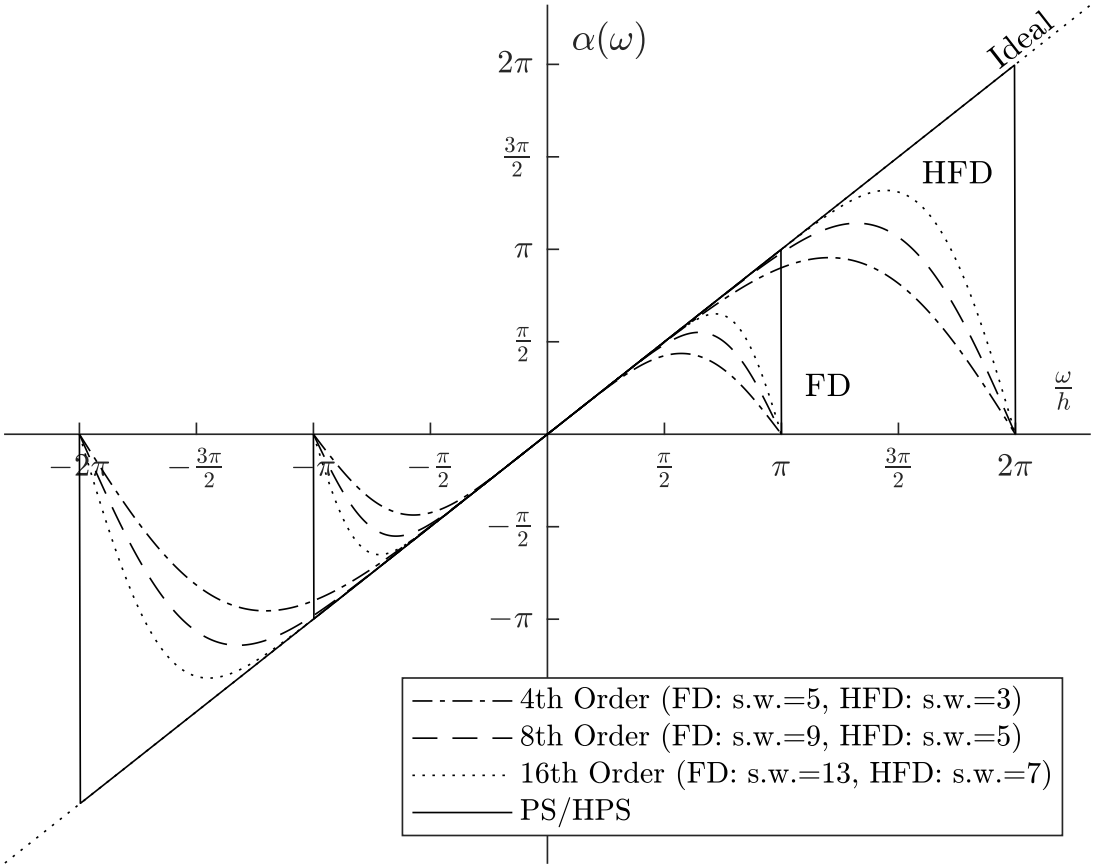

Fig. 5.4: The graphical representation of $\alpha(\omega)$ for FD/PS and HFD/HPS compared to the ideal case $\alpha(\omega) = \omega$.

Figure 5.4 shows how well $\alpha(\omega)$ is approximated for various values of ω at different orders of convergence for FD and HFD methods along with their respective limits PS and HPS. As expected PS and HPS capture exactly all the Fourier modes in the region of validity for the respective method. This also illustrates why HFD reduces trailing waves due to how much closer the HFD curves follow the ideal curve in the region where standard FD is valid [4]. Another attribute to consider is points per wavelength (PPW) in the context of solving (5.1). PPW is discussed in [1], where HFD are found to require half the PPW compared to their FD counterparts. Similarly, HPS requires half the PPW as PS.

5.4 Time stepping The stability constraint for explicit time steppers introduced by discretizing (5.1) or (5.2) using FD or HFD (respectively) in space scales like $\mathcal{O}\left(\frac{k}{h}\right)$ where k is the time step and h is the spatial node spacing [1]. The semi-discrete version of (5.1) when using the PS convolution approach can be written,

$$\begin{bmatrix} \vdots \\ \hat{u}_k \\ \vdots \end{bmatrix}_t = - \begin{bmatrix} \ddots & & 0 \\ & i\hat{w}_k & \\ 0 & & \ddots \end{bmatrix} \begin{bmatrix} \vdots \\ \hat{u}_k \\ \vdots \end{bmatrix} \tag{5.3}$$

where $\hat{w}_k$ are the standard wave-numbers $\left[0, 1, \cdots, \frac{N-1}{2}, -\frac{N-1}{2}, \cdots, -1\right]$. Likewise, when using HPS on (5.2)

$$\left[\begin{array}{c} \vdots \\ \hat{u}_k \\ \vdots \\ \hline \vdots \\ \hat{v}_k \\ \vdots \end{array}\right]_t = - \left[\begin{array}{ccc|ccc} & 0 & & 1 & & 0 \\ & & & & \ddots & \\ & & & 0 & & 1 \\ \hline \ddots & & 0 & \ddots & & 0 \\ & \hat{c}_k & & & i\hat{d}_k & \\ 0 & & \ddots & 0 & & \ddots \end{array}\right] \left[\begin{array}{c} \vdots \\ \hat{u}_k \\ \vdots \\ \hline \vdots \\ \hat{v}_k \\ \vdots \end{array}\right] \tag{5.4}$$

where $\hat{c}_k$ and $\hat{d}_k$ are defined in (4.8). While one won't conduct these matrix multiplications in practice using sparse matrices, as illustrated in (5.3) and (5.4), this matrix formulation gives insights into the stability constraint. The eigenvalues in (5.3) grow like $\mathcal{O}(N)$ indicating the stability constraint is $\mathcal{O}\left(\frac{k}{h}\right)$. In a similar argument made in [1, 4] via a similarity transform, the eigenvalues of the matrix in (5.4) grow like $\mathcal{O}(N)$ again indicating the stability constraint is $\mathcal{O}\left(\frac{k}{h}\right)$ while also showing the eigenvalues are purely imaginary. While both PS and HPS discretization introduce similar stability constraints for explicit time steppers, it is worth noting that HPS still requires roughly half the time step size for the same number of total nodes N in space. Heuristically, this seems obvious as twice as much information is being utilized.

5.5 Variable coefficient transport Here we consider a spatially dependent wave speed problem

$$\frac{\partial u}{\partial t} + a(x)\frac{\partial u}{\partial x} = 0 \tag{5.5}$$

where $a(x) = (10 - 9\cos(x))^{-1}$ and test against the closed form solution $u(x,t) = \left[\cos\left(\frac{1}{20}\left(t - 10x + 9\sin(x)\right)\right)\right]^{20}$ shown in Figure 5.5. This illustrates the convergence of the periodic HPS scheme on a time dependent PDE in comparison with standard the PS method. To eliminate the effects of numerical time-steppers in order to purely focus on errors caused by PS and HPS, we consider the linear semi-discrete problem

$$\begin{bmatrix} \vdots \\ u_k \\ \vdots \end{bmatrix}_t = - \begin{bmatrix} \quad \\ \mathbf{D} \\ \quad \end{bmatrix} \begin{bmatrix} \vdots \\ u_k \\ \vdots \end{bmatrix} \tag{5.6}$$

where the differentiation matrix $\mathbf{D}$ represents the linear spatial operator acting on the vector u. Given that $\mathbf{D}$ has eigenvalue decomposition $\mathbf{D} = \mathbf{V}\mathbf{\Lambda}\mathbf{V}^{-1}$, the solution to (5.6) at a given time t with initial condition u_0 can be written $u = -\mathbf{V}e^{\mathbf{\Lambda} t}\mathbf{V}^{-1}u_0$ where $\mathbf{V}$ is the matrix comprised of the eigenvectors of $\mathbf{D}$ and $\mathbf{\Lambda}$ is the diagonal matrix comprised of the eigenvalues of $\mathbf{D}$.

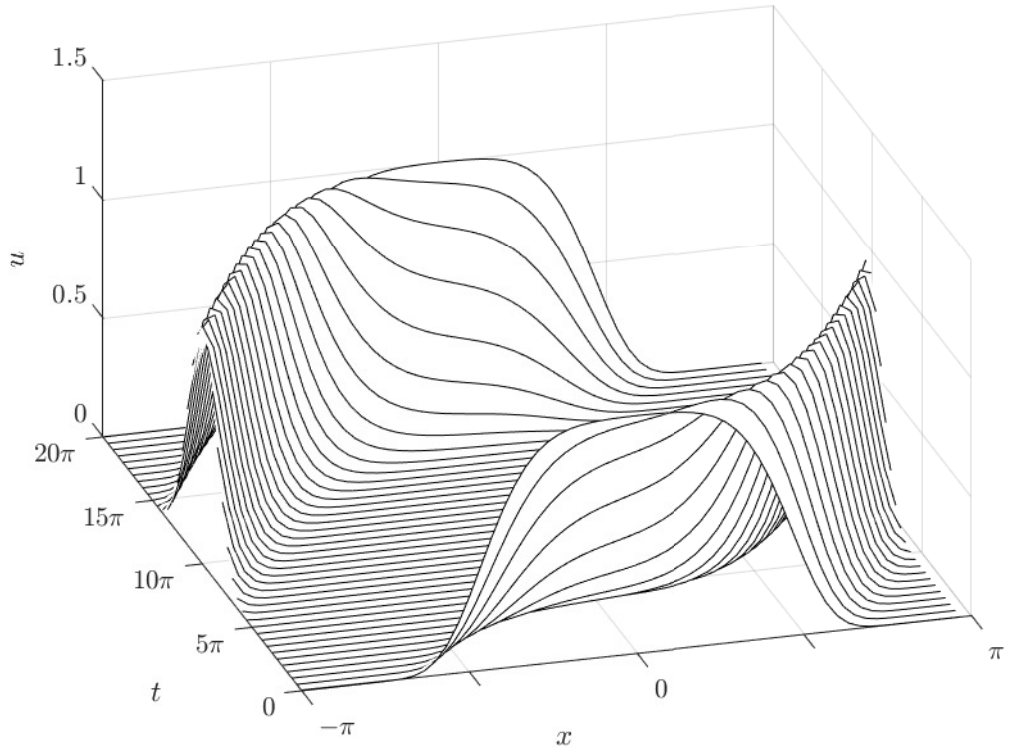

Fig. 5.5: Numerical solution of (5.5) using HPS with $N = 60$ over one revolution using the eigenvalue decomposition solution (visually indistinguishable from the analytic solution).

Figure 5.5 shows the numerical solution of (5.5) over one revolution when discretizing in space with HPS with $N = 60$ nodes. Figure 5.6 shows the accumulation of error over 50 revolutions when using either the PS or HPS approximation in space. HPS used 60 nodes in space while PS used 121 nodes (due to the odd number restriction). For roughly the half number of nodes in space the accuracy of HPS is comparable to PS. Figure 5.7 shows this same calculations, but when both PS and HPS use the same $N = 61$ nodes. Since HPS converges roughly twice as fast as PS we certainly expect HPS to outperform given the same node count, however, requiring roughly twice the number of operations. This might however be off-set by HPS being better able to utilize two cores in parallel.

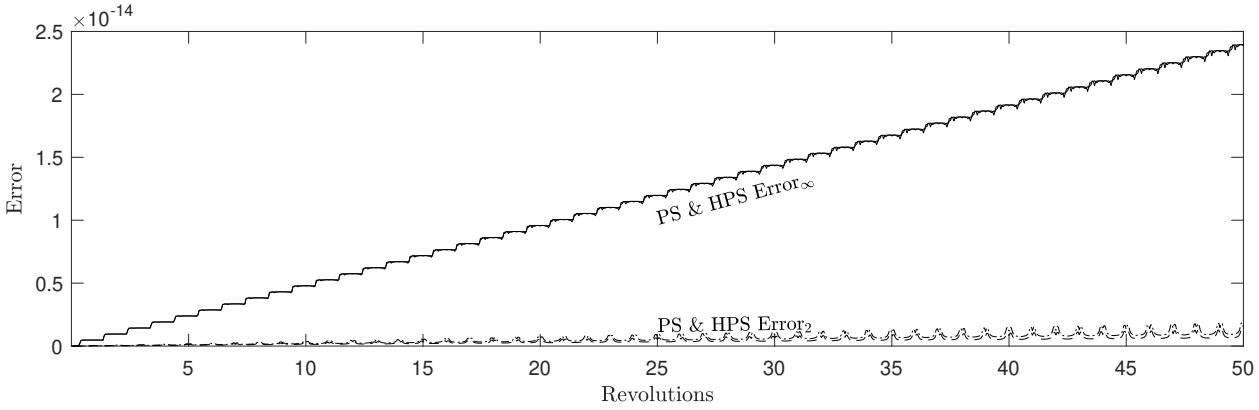

Fig. 5.6: The ∞-norm and normalized ℓ_2-norm errors over 50 revolutions while using PS ($N = 121$) and HPS ($N = 60$) when solving (5.5) using the eigenvalue decomposition solution. Note that the errors rise the fastest around half-integer values of the number of revolutions, i.e. when the traveling pulse is the narrowest (see Figure 5.5).

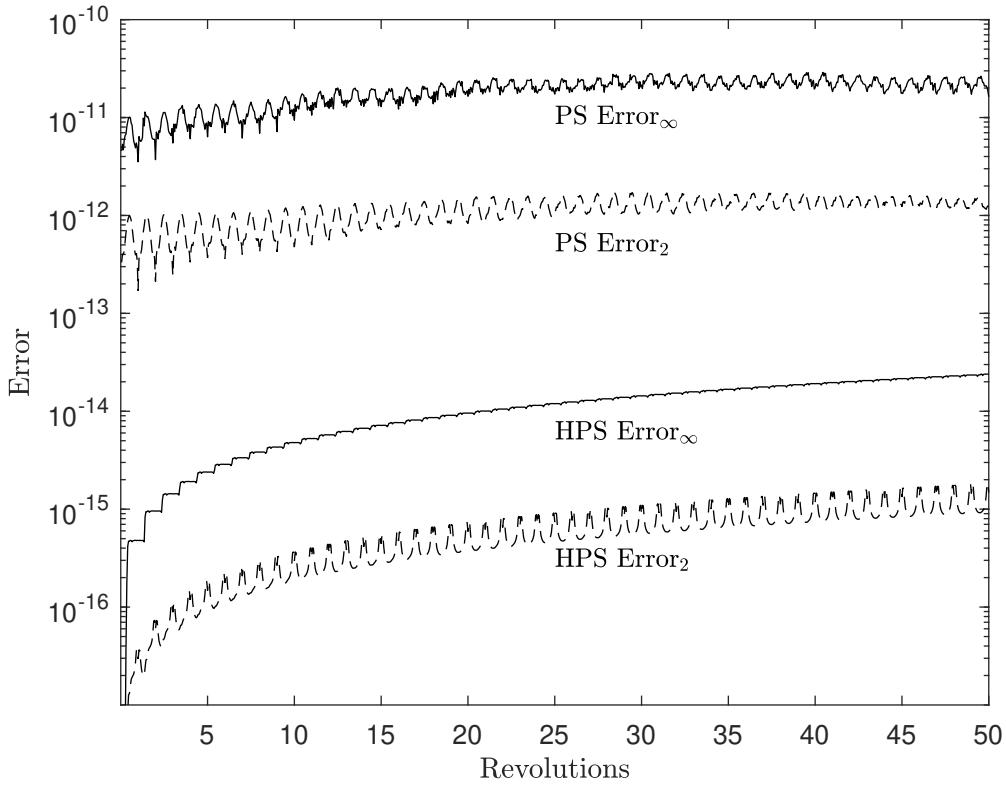

Fig. 5.7: Semi-log plot of The ∞-norm and normalized ℓ_2-norm errors over 50 revolutions while using PS and HPS with both using $N = 61$ nodes when solving (5.5) using the eigenvalue decomposition solution.

6 Conclusions By using both function and first derivative information, HPS provides an alternative approach to the standard PS method with some of the following benefits:

1. given a smooth enough first derivative in space, a HPS approximation using N nodes roughly matches the PS approximation accuracy when using $2N$ nodes
2. a seemingly more 'local' approximation of differential operators due to faster decay rates of coefficients on function values.
3. a doubling of the interval of the accuracy representation of the Fourier modes from $[-\frac{\pi}{h}, \frac{\pi}{h}]$ to $[-\frac{2\pi}{h}, \frac{2\pi}{h}]$
4. no major consequence in the time stepping stability constraint by introducing higher derivatives via differentiation of the PDE.

One possible further advantage with the HPS method concerns the use of multiple cores for parallel processing. When time stepping the wave equation (or nonlinear equations, like the Korteweg-de Vries equation) it becomes difficult to utilize more than a single core using the standard PS method. However, the HPS method divides these computations into two separate calculations, opening the possibility to run these processes in parallel. This advantage potentially increases if higher derivatives are included into the HPS method (although this paper only discusses up to the first derivative), possibly allowing still more cores to be utilized.

The key present novelty lies in establishing Hermite-PS formulas, generalizing 'classical' PS formulas, and giving numerous closed form expressions for these. The HPS vs. PS wave equation test described here give results in line with more extensive HFD vs. FD tests, for the Korteweg-de Vries and 2-D wave equations in [1] and [4], respectively.

Continuation of this work could include application to nonlinear PDEs, the study of possible speed up by utilizing multiple cores, and the introduction of higher derivative terms in the HPS approximation.

REFERENCES

[1] D. Abrahamsen and B. Fornberg, *Solving the Korteweg-de Vries equation with Hermite-based finite differences*, Submitted (2020).

[2] B. Fornberg, *High-order finite differences and the pseudospectral method on staggered grids*, SIAM Journal on Numerical Analysis **27** (1990), no. 4, 904–918.

[3] ———, *A Practical Guide to Pseudospectral Methods*, vol. 1, Cambridge University Press, 1998.

[4] ———, *An algorithm for calculating Hermite-based finite difference weights*, IMA Journal of Numerical Analysis (2020).

[5] D. Gottlieb and S.A. Orszag, *Numerical Analysis of Spectral Methods: Theory and Applications*, vol. 26, SIAM, 1977.

[6] Advanpix, Multiprecision Computing Toolbox for MATLAB, Advanpix LLC., Yokohama, Japan.

[7] L.N. Trefethen, *Spectral methods in MATLAB*, vol. 10, SIAM, 2000.

[8] J. A. Weideman and S.C. Reddy, *A MATLAB differentiation matrix suite*, ACM Transactions on Mathematical Software (TOMS) **26** (2000), no. 4, 465–519.

7 Appendix A: Brief tables for centered FD, HFD, and HPS approximations

This section contains tables that contain the coefficients for FD, HFD, and HPS used to approximate various derivatives.

Order of		Approximations at $x = 0$; x coordinates at nodes								
deri-vative	accu-racy	-4	-3	-2	-1	0	1	2	3	4
0	∞					1				
1	2				$-\frac{1}{2}$	0	$\frac{1}{2}$			
	4			$\frac{1}{12}$	$-\frac{2}{3}$	0	$\frac{2}{3}$	$-\frac{1}{12}$		
	6		$-\frac{1}{60}$	$\frac{3}{20}$	$-\frac{3}{4}$	0	$\frac{3}{4}$	$-\frac{3}{20}$	$\frac{1}{60}$	
	8	$\frac{1}{280}$	$-\frac{4}{105}$	$\frac{1}{5}$	$-\frac{4}{5}$	0	$\frac{4}{5}$	$-\frac{1}{5}$	$\frac{4}{105}$	$-\frac{1}{280}$
2	2				1	-2	1			
	4			$-\frac{1}{12}$	$\frac{4}{3}$	$-\frac{5}{2}$	$\frac{4}{3}$	$-\frac{1}{12}$		
	6		$\frac{1}{90}$	$-\frac{3}{20}$	$\frac{3}{2}$	$-\frac{49}{18}$	$\frac{3}{2}$	$-\frac{3}{20}$	$\frac{1}{90}$	
	8	$-\frac{1}{560}$	$\frac{8}{315}$	$-\frac{1}{5}$	$\frac{8}{5}$	$-\frac{205}{72}$	$\frac{8}{5}$	$-\frac{1}{5}$	$\frac{8}{315}$	$-\frac{1}{560}$
3	2			$-\frac{1}{2}$	1	0	-1	$\frac{1}{2}$		
	4		$\frac{1}{8}$	-1	$\frac{13}{8}$	0	$-\frac{13}{8}$	1	$-\frac{1}{8}$	
	6	$-\frac{7}{240}$	$\frac{3}{10}$	$-\frac{169}{120}$	$\frac{61}{30}$	0	$-\frac{61}{30}$	$\frac{169}{120}$	$-\frac{3}{10}$	$\frac{7}{240}$
4	2			1	-4	6	-4	1		
	4		$-\frac{1}{6}$	2	$-\frac{13}{2}$	$\frac{28}{3}$	$-\frac{13}{2}$	2	$-\frac{1}{6}$	
	6	$\frac{7}{240}$	$-\frac{2}{5}$	$\frac{169}{60}$	$-\frac{122}{15}$	$\frac{91}{8}$	$-\frac{122}{15}$	$\frac{169}{60}$	$-\frac{2}{5}$	$\frac{7}{240}$

Table 7.1: Weights for some centered FD formulas on a unit-spaced grid, giving approximations to $f^{(k)}(x)|_{x=0}$, $k = 0, 1, \ldots, 4$. This table contains the same information as Table 3.1-1 in [3] and Table B1 in [4].

Weights for	Order of derivative	Order of accuracy	Approximations at $x=0$; x coordinates at nodes								
			-4	-3	-2	-1	0	1	2	3	4
$f(x_i)$	0	∞					1				
	1	∞					0				
	2	4				2	-4	2			
		8			$\frac{7}{54}$	$\frac{64}{27}$	-5	$\frac{64}{27}$	$\frac{7}{54}$		
		12		$\frac{157}{18000}$	$\frac{69}{250}$	$\frac{39}{16}$	$-\frac{49}{9}$	$\frac{39}{16}$	$\frac{69}{250}$	$\frac{157}{18000}$	
		16	$\frac{199}{343000}$	$\frac{11824}{385875}$	$\frac{48}{125}$	$\frac{304}{125}$	$-\frac{205}{36}$	$\frac{304}{125}$	$\frac{48}{125}$	$\frac{11824}{385875}$	$\frac{199}{343000}$
	3	4				$-\frac{15}{2}$	0	$\frac{15}{2}$			
		8			$-\frac{31}{144}$	$-\frac{88}{9}$	0	$\frac{88}{9}$	$\frac{31}{144}$		
		12		$-\frac{167}{18000}$	$-\frac{963}{2000}$	$-\frac{171}{16}$	0	$\frac{171}{16}$	$\frac{963}{2000}$	$\frac{167}{18000}$	
		16	$-\frac{2493}{5488000}$	$-\frac{12944}{385875}$	$-\frac{87}{125}$	$-\frac{1392}{125}$	0	$\frac{1392}{125}$	$\frac{87}{125}$	$\frac{12944}{385875}$	$\frac{2493}{5488000}$
$f'(x_i)$	0	∞					0				
	1	∞					1				
	2	4				$\frac{1}{2}$	0	$-\frac{1}{2}$			
		8			$\frac{1}{36}$	$\frac{8}{9}$	0	$-\frac{8}{9}$	$-\frac{1}{36}$		
		12		$\frac{1}{600}$	$\frac{9}{100}$	$\frac{9}{8}$	0	$-\frac{9}{8}$	$-\frac{9}{100}$	$-\frac{1}{600}$	
		16	$\frac{1}{9800}$	$\frac{32}{3675}$	$\frac{4}{25}$	$\frac{32}{25}$	0	$-\frac{32}{25}$	$-\frac{4}{25}$	$-\frac{32}{3675}$	$-\frac{1}{9800}$
	3	4				$-\frac{3}{2}$	-12	$-\frac{3}{2}$			
		8			$-\frac{1}{24}$	$-\frac{8}{3}$	-15	$-\frac{8}{3}$	$-\frac{1}{24}$		
		12		$-\frac{1}{600}$	$-\frac{27}{200}$	$-\frac{27}{8}$	$-\frac{49}{3}$	$-\frac{27}{8}$	$-\frac{27}{200}$	$-\frac{1}{600}$	
		16	$-\frac{3}{39200}$	$-\frac{32}{3675}$	$-\frac{6}{25}$	$-\frac{96}{25}$	$-\frac{205}{12}$	$-\frac{96}{25}$	$-\frac{6}{25}$	$-\frac{32}{3675}$	$-\frac{3}{39200}$

Table 7.2: Weights for some centered HFD formulas on a unit-spaced grid. Applied to $f(i)$ and $f'(i)$ values with i integers centered around the origin, they give approximations (at $x=0$) to $f^{(k)}(x)|_{x=0}$, $k=0,1,\ldots,3$. If the grid has spacing h, the $f(i)$ weights for the second derivative should be divided by h^2, for the third derivative by h^3, etc., with one power of h less for the $f'(i)$ weights. This table contains the same information as Table B2 in [4].

$p=$	2	3	4
a_0	$-\frac{2\pi^2}{3}$	0	$\frac{16\pi^4}{15}$
a_k	$\frac{2}{k^2}$	$-\frac{12}{k^3}$	$\frac{72-8k^2\pi^2}{k^4}$
b_0	0	$-2\pi^2$	0
b_k	$-\frac{2}{k}$	$\frac{6}{k^2}$	$\frac{8(k^2\pi^2-3)}{k^3}$
c_0	$-\frac{2(N^2-1)\pi^2}{3N^2}$	0	$\frac{8(3-5N^2+2N^4)\pi^4}{15N^4}$
c_k	$\frac{2\pi^2\csc\left(\frac{k\pi}{N}\right)}{N^2}$	$-\frac{12\pi^3\cot\left(\frac{k\pi}{N}\right)\csc^2\left(\frac{k\pi}{N}\right)}{N^3}$	$-\frac{8\pi^4\csc^2\left(\frac{k\pi}{N}\right)\left(6+N^2-9\csc^2\left(\frac{k\pi}{N}\right)\right)}{N^4}$
d_0	0	$-\frac{2(N^2+1)\pi^2}{N^2}$	0
d_k	$-\frac{2\pi\cot\left(\frac{k\pi}{N}\right)}{N}$	$\frac{6\pi^2\csc^2\left(\frac{k\pi}{N}\right)}{N^2}$	$\frac{8\pi^3\cot\left(\frac{k\pi}{N}\right)\left(N^2-3\csc^2\left(\frac{k\pi}{N}\right)\right)}{N^3}$
$\hat{c}_k$	$\frac{4k(k-N)\pi^2}{N^2}$	$\frac{8ik(2k^2-3kN+N^2)\pi^3}{N^3}$	$-\frac{16k(k-N)(3k^2-3kN+N^2)\pi^4}{N^4}$
$\hat{d}_k$	$\left(\frac{4k}{N}-2\right)\pi$	$\frac{4i(3k^2-3kN+N^2)\pi^2}{N^2}$	$-\frac{8(k^4-(k-N)^4)\pi^3}{N^4}$

Table 7.3: HPS coefficients for various implementations given a fixed derivative order p. On an infinite interval of unit spacing a_0 and a_k are used on f and b_0 and b_k are used on f'. On a periodic interval with N nodes of unit spacing c_0 and c_k are used on f and d_0 and d_k and used on f'. While using convolutions on a periodic interval with N nodes of unit spacing $\hat{c}_k$ is applied to $\hat{f}$ and d_k is applied to $\hat{f}'$.

7.1 Dispersion for HFD Consider the standard 1-D transport equation

$$\frac{\partial u}{\partial t}+\frac{\partial u}{\partial x}=0 \tag{7.1}$$

with the single Fourier mode solution $u(x,t)=e^{i\omega x-i\alpha(\omega)t}$. Analytically, it should hold that $\alpha(\omega)=\omega$. HFD can be applied to (7.1) by differentiating once in space, as considered in [4]. By substituting the single Fourier mode solution into (7.1) or the appropriate system for HFD and discretely approximating any spatial derivatives a relation for $\alpha(\omega)$ can be found [1]. These functions $\alpha(\omega)$ as shown in Figure 5.4 and can help explain the doubling of the region where the Fourier modes are represented.

[1] For example, in the FD, order $p=4$ case, one obtains $\alpha(\omega)=\frac{1}{ih}\left(\frac{1}{12}e^{-2i\omega h}-\frac{2}{3}e^{-i\omega h}+\frac{2}{3}e^{i\omega h}-\frac{1}{12}e^{2i\omega h}\right)=\frac{4}{3h}\sin(\omega h)-\frac{1}{6h}\sin(2\omega h)=\omega-\frac{h^4\omega^5}{30}+\frac{h^6\omega^7}{252}+\cdots$.

Scheme	Order	$\alpha(\omega)$
FD	4	$\omega - \frac{h^4\omega^5}{30} + \frac{h^6\omega^7}{252} + \cdots$
	8	$\omega - \frac{h^8\omega^9}{630} + \frac{h^{10}\omega^{11}}{2310} + \cdots$
	12	$\omega - \frac{h^{12}\omega^{13}}{12012} + \frac{h^{14}\omega^{15}}{27720} + \cdots$
	16	$\omega - \frac{h^{16}\omega^{17}}{218790} + \frac{h^{18}\omega^{19}}{366795} + \cdots$
HFD	4	$\omega - \frac{h^4\omega^5}{1080} - \frac{h^6\omega^7}{54432} + \cdots$
	8	$\omega - \frac{h^8\omega^9}{441000} - \frac{h^{10}\omega^{11}}{22638000} + \cdots$
	12	$\omega - \frac{h^{12}\omega^{13}}{155387232} - \frac{h^{14}\omega^{15}}{7888890240} + \cdots$
	16	$\omega - \frac{h^{16}\omega^{17}}{50684891400} - \frac{h^{18}\omega^{19}}{2549151891000} + \cdots$

Table 7.4: The $\alpha(\omega)$ relationship for standard FD and HFD for varying orders.

Table 7.4 shows the series expansions of the $\alpha(\omega)$ function for standard FD and HFD. These functions can also be seen in part in Figure 5.4